JCTC Journal of Chemical Theory and Computation

Article

Cite This: J. Chem. Theory Comput. 2018, 14, 1523−1533

pubs.acs.org/JCTC

Rovibrational Resonances in H_2He^+

Dóra Papp,[†] Attila G. Császár,[†] Kaoru Yamanouchi,[‡] and Tamás Szidarovszky*[,†]

[†]Laboratory of Molecular Structure and Dynamics, Institute of Chemistry, Eötvös Loránd University and MTA-ELTE Complex Chemical Systems Research Group, Pázmány Péter sétány 1/A, H-1117 Budapest, Hungary

[‡]The University of Tokyo, 7-3-1 Hongo, Bunkyo-ku, Tokyo 113-0033, Japan

Supporting Information

ABSTRACT: The nuclear dynamics of the metastable H_2He^+ complex is explored by symmetry considerations and angular momentum addition rules as well as by accurate quantum chemical computations with complex coordinate scaling, complex absorbing potential, and stabilization techniques. About 200 long-lived rovibrational resonance states of the complex are characterized and selected long-lived states are analyzed in detail. The stabilization mechanism of these long-lived resonance states is discussed on the basis of probability density plots of the wave functions. Overlaps of wave functions derived by a reduced-dimensional model with the full-dimensional wave functions reveal dissociation pathways for the long-lived resonance states and allow the calculation of their branching ratios.

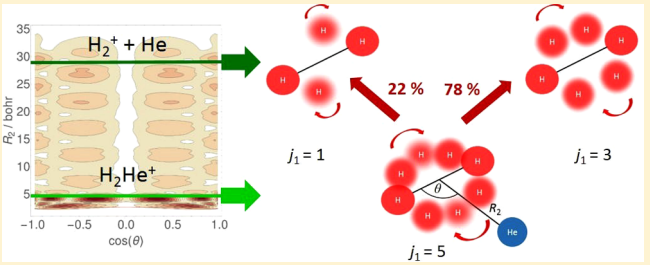

1. INTRODUCTION

H_2He^+, composed of the two most abundant elements of our known universe, can be regarded as a collisional complex appearing in the course of the bimolecular reactions $H_2^+ + He \rightarrow HeH^+ + H$ and $HeH^+ + H \rightarrow H_2^+ + He$. The H_2He^+ complex is expected to play a fundamental role in the formation and consumption of HeH^+ in the chemical reactions in the premordial gas.[1,2] The collisional cross sections of the above two reactions have been determined both experimentally[3−6] and computationally,[6−8] whereby the theoretical works use accurate potential energy surfaces (PES) on which the investigated scatterings proceed.

Existence of H_2He^+ has also been considered in the interstellar medium, and theoretical studies[9−11] have been carried out for facilitating the spectroscopic detection of H_2He^+ in outer space. The bound and quasibound rovibrational levels of H_2He^+ as well as absorption and emission spectra corresponding to its bound rovibrational levels have been computed and reported.[9−12] As to the experimental side, only one report has been published on the rovibrational spectrum of H_2He^+,[13] in which three microwave transitions and their fine structures were reported.

It has also been shown theoretically that H_2He^+ can be formed through the radiative association reaction $H_2^+(^2\Sigma_g^+) + He \rightarrow [H_2^+(^2\Sigma_g^+)−He] + h\nu$,[14,15] as well as through the radiative charge transfer reaction $H_2(^1\Sigma_g^+) + He^+ \rightarrow [H_2^+(^2\Sigma_g^+)−He] + h\nu$, in which a positive charge is transferred from He^+ to H_2.[16]

In all these collision and association reactions, the characters of the rovibrational states of H_2He^+ embedded in the dissociation continua, which are also referred to as quasibound or resonance states, govern the dynamics. Such resonance states, whose lifetimes can be many orders of magnitude longer than the time scale of scattering processes without intermediate resonances, can appear as peak profiles in the scattering cross sections and can lead to a significant increase in continuum-bound radiative association processes. Indeed, while initially the rate of the radiative association reaction $H_2^+ + He \rightarrow H_2He^+$ was considered to be too small for astrophysical implications, it was found that the contribution of this reaction could not be neglected because of the presence of the rovibrational resonance states of H_2He^+.[14]

Furthermore, the rotational cooling of H_2^+ by collisions with a cold He buffer gas is enhanced significantly by resonance states of H_2He^+.[8] Recently it was also emphasized that the ultrafast vibration and dissociation dynamics of H_2He^+ in the presence of intense laser fields is influenced by the rovibrational resonance states of H_2He^+.[17]

In order to understand quantitatively the rich dynamical processes in which H_2He^+ is involved in, it is necessary to understand the rovibrational level structure of the complex both below and above dissociation. In the present study, we perform accurate variational computations of the bound and resonance rovibrational states of H_2He^+. Based on the resultant energies and lifetimes of the rovibrational states, as well as the branching ratios of the decay channels, we discuss the physical origin of long-lived rovibrational resonance states and assign quantum numbers to them. We also explore the energy region above the first and the second dissociation asymptotes to find bound states by taking advantage of molecular symmetry. Furthermore, we show that for this molecular cation the nuclear dynamics above dissociation can be understood and predicted by simple angular momentum addition rules, taking into account the rotational angular momentum of the H_2^+ moiety and the

Received: November 14, 2017
Published: February 1, 2018

DOI: 10.1021/acs.jctc.7b01136
J. Chem. Theory Comput. 2018, 14, 1523−1533

angular momentum of the "pseudodiatomic" unit composed of He and the center of mass of H_2^+.

2. THEORETICAL AND COMPUTATIONAL DETAILS

2.1. Potential Energy Surface. Our theoretical investigation of the bound and resonance rovibrational states of H_2He^+ is based on the so-called MRCI8 PES of ref 7. The MRCI8 PES of the ground electronic state of H_2He^+, to the best of our knowledge, is the most accurate one available. Two in-house program packages, D^{2}FOPI-CCS[18−20] and GENIUSH-CAP,[21−24] were employed to compute the bound and resonance rovibrational states of H_2He^+ supported by the MRCI8 PES.

2.2. D^{2}FOPI-CCS. One of the variational nuclear-motion program packages employed in this work is D^{2}FOPI.[18] D^{2}FOPI is a discrete variable representation (DVR)[25]-based quasivariational code designed for computing bound rovibrational states of triatomic molecules with high precision and accuracy. The extension of D^{2}FOPI allowing the computation of resonance states utilizes the complex coordinate scaling (CCS)[19] method. The theoretical approach of the D^{2}FOPI-CCS protocol used in this work is identical to that described in ref 20.

As a first step during the computation of rovibrational resonances, all the bound rovibrational states and hundreds of eigenvectors and eigenenergies above the first dissociation threshold are computed using D^{2}FOPI. Then these eigenstates, or a subset of them, are used as basis functions to construct the matrix representation of the complex-coordinate-scaled rovibrational Hamiltonian. The resulting complex symmetric Hamiltonian is diagonalized, and its complex eigenvalues are plotted on the complex plane. Repeating this procedure for many different values of the complex scaling parameter, eigenvalue trajectories are formed on the complex plane, in which cusps or similar features[26] identify the resonance eigenvalues.

For all D^{2}FOPI and D^{2}FOPI-CCS computations, the Jacobi coordinate system,[27] presented in Figure 1, was adopted. Further technical details can be found in the Supporting Information.

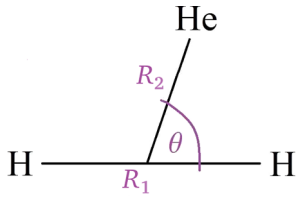

Figure 1. Jacobi coordinate system of H_2He^+. The MRCI8[7] PES supports two equivalent linear equilibrium structures at (R_1,R_2,θ) = (2.09 bohr, 2.96 bohr, 0) and (2.09 bohr, 2.96 bohr, π).

2.3. GENIUSH-CAP. The second program package employed for nuclear-motion computations in this study is GENIUSH.[21,22] GENIUSH was used to determine bound rovibrational levels of the H_2He^+ system, while GENIUSH-CAP,[23,24] an extended version of GENIUSH, was employed for the rovibrational resonance computations. GENIUSH computes rovibrational bound states by numerically representing not only the potential but also the kinetic energy operator of a molecular system in user-specified internal coordinates. In GENIUSH, an iterative Lanczos eigensolver is used to determine the desired eigenvalues and eigenvectors without any explicit constraints on the number of atoms in the molecule. Reduced-dimensional models of the molecules investigated can easily be defined within the framework of the GENIUSH protocol.

GENIUSH-CAP is an extension of GENIUSH, in which a complex absorbing potential (CAP)[28−31] is added to the standard rovibrational Hamiltonian, and the matrix representation of the CAP-perturbed Hamiltonian is constructed using the basis of the eigenvectors of the unperturbed Hamiltonian. The resulting complex symmetric Hamiltonian matrix is diagonalized at several hundred different values of the CAP-strength parameter[23,28] and the eigenvalues thus obtained are plotted on the complex plane. Along the trajectories formed, cusps are associated with resonance energies and lifetimes.

In order to assign quantum numbers to the vibrational resonances of H_2He^+ and derive the branching ratios of the dissociation channels starting from these resonances, overlaps between the full-dimensional GENIUSH-CAP resonance states and appropriate reduced-dimensional GENIUSH eigenstates were computed. The reduced-dimensional GENIUSH computations were carried out by fixing the R_2 coordinate at 80.0 bohr, while for the R_1 and θ coordinates the same DVR grid was employed as in the full-dimensional computations. Overlaps between the full-dimensional GENIUSH-CAP resonance states and the reduced-dimensional GENIUSH eigenstates were computed at several fixed R_2 values of the full-dimensional eigenstates.

Further technical details can be found in the Supporting Information.

2.4. Stabilization Computations. The GENIUSH code has also been employed to carry out computations yielding resonances according to the stabilization method.[19,32,33] The stabilization method involves the monitoring of eigenvalues above the first dissociation asymptote, which are obtained from several standard Hermitian computations with slightly different ranges along the R_2 dissociation coordinate. The results can most easily be visualized in the form of a histogram. In the stabilization histogram the eigenvalues computed at different R_2 ranges that fall in the respective bins are counted, and each clear peak located above the dissociation threshold represents an eigenvalue which is converged well, showing that a resonance energy was obtained.[32,33]

Further technical details can be found in the Supporting Information.

2.5. Wave Function and Probability Density Plots. All the plots of the wave functions presented in this article depict the DVR basis coefficients, and all the plots for the probability densities depict the absolute values of the DVR basis coefficients, as detailed in ref 23. The plots obtained with the DVR coefficients represent the same nodal structure as the plots of the wave functions.

3. RESULTS AND DISCUSSION

3.1. Dissociation Channels: Role of Symmetry and Angular Momentum. Before examining in detail the accurate numerical results concerning the rovibrational dynamics of H_2He^+ below and above the dissociation threshold energy, it is worth examining possible dissociation channels of the system on the basis of symmetry considerations.

The molecular symmetry group of H_2He^+ is the S_2^* or $C_{2v}(M)$ group[34] (Table 1). The spatial wave functions of all rovibrational states of H_2He^+ must transform according to one of the irreducible representations of $C_{2v}(M)$. Furthermore, under field-free conditions, each level can be labeled with the good quantum numbers J and $p \in \{1, -1\}$, where p denotes parity. It is clear from Table 1 that the A_1 and B_2 irreducible representations of $C_{2v}(M)$ belong to $p = 1$, while A_2 and B_1 belong to

DOI: 10.1021/acs.jctc.7b01136
J. Chem. Theory Comput. 2018, 14, 1523−1533

Table 1. Character Table of the $C_{2v}(M)$ and the Equivalent S_2^* Molecular Symmetry Groups[a]

$C_{2v}(M)$	S_2^*	E	(12)	E^*	(12)*
A_1	A^+	1	1	1	1
A_2	A^-	1	1	−1	−1
B_1	B^-	1	−1	−1	1
B_2	B^+	1	−1	1	−1
Γ		1	$(-1)^{j_1}$	$(-1)^{j_1+j_2}$	$(-1)^{j_2}$

[a]Operations E, (12), E^*, and (12)* stand for identity, permutation of the two identical nuclei, spatial inversion, and permutation with inversion, respectively. The bottom row shows the Γ representation spanned by the complete spatial wave function of H_2He^+ characterized by j_1 and j_2, where j_1 represents the rotational quantum number for the rotational motion of the H_2^+ moiety and j_2 represents the rotational quantum number for the rotational motion of the "pseudodiatomic" unit composed of He and the center of mass of H_2^+.

$p = -1$. Table 1 also shows that A_1 and A_2 correspond to *para*-H_2He^+, while B_1 and B_2 correspond to *ortho*-H_2He^+.

Although H_2He^+ is an open-shell molecular cation, we use the integer values of the rotational angular momentum for J since the electronic spin does not influence the nuclear dynamics treated in the present study. The total rotational angular momentum is the sum of the $\hat{j}_1$ angular momentum of the H_2^+ moiety and the $\hat{j}_2$ angular momentum for the relative motion of the H_2^+ center of mass and He, i.e.,

$$\hat{J} = \hat{j}_1 + \hat{j}_2, J \in \{|j_1 - j_2|, ..., j_1 + j_2\} \quad (1)$$

When describing the H_2He^+ complex, j_1 and j_2 are approximately good quantum numbers since many combinations of j_1 and j_2, all of which correspond to a given J, can contribute to a single rovibrational eigenstate because of the PES-induced couplings between the angular momentum wave functions of the different j_1 and j_2 values. However, when considering the dissociation products of a given dissociation channel, appearing in the asymptotic regions of the PES, the spatial wave function of the full system can be written as the product of the angular momentum wave functions represented by j_1 and j_2. Within this approach, the symmetry of the complete wave function, transforming as one of the irreducible representations of the $C_{2v}(M)$ group, can be specified by j_1 and j_2. Considering the definitions of j_1 and j_2, we can show on the basis of the transformation properties of the spherical harmonics that upon the (12) permutation of the two H atoms the complete spatial wave function acquires a $(-1)^{j_1}$ factor, the E^* spatial inversion leads to a factor of $(-1)^{j_1+j_2}$, and the (12)* permutation with inversion gives a factor of $(-1)^{2j_1+j_2} = (-1)^{j_2}$.

On the PES of the electronic ground state, the lowest dissociation energy D_0 of H_2He^+ having $J = 0$ is the dissociation energy of the reaction $H_2He^+ \rightarrow H_2^+ + He$, whereby H_2^+ is in its ground rovibrational state, $j_1 = 0$ and $v_{H_2^+} = 0$. Because of eq 1, $j_2 = 0$ in this case. The first dissociation energy corresponding to the MRCI8 PES of ref 7 is $D_0 = 1775.42$ cm^{-1}. Additional dissociation channels corresponding to the decomposition reaction $H_2He^+ \rightarrow H_2^+ + He$ can be opened by increasing J, j_1, or $v_{H_2^+}$. First, we only consider the rotational excitation by increasing J and j_1. For a given J, the energy of the dissociation channels labeled with j_1 can be expressed by the rigid-rotor energy formula of $Bj_1(j_1 + 1)$, where $B = 30.2$ cm^{-1} corresponds to the rotational constant of the H_2^+ moiety.[35]

According to eq 1, $j_1 = j_2$ should hold in the case of $J = 0$. Therefore, as shown in Table 1, only $p = 1$ states, having A_1 or B_2 symmetry, are allowed. For A_1 symmetry levels, j_1 must be even, while for B_2 symmetry states j_1 must be odd. Consequently, the lowest-energy dissociation channel, characterized by the quantum numbers $J = j_1 = j_2 = 0$, is accessible only for states with A_1 symmetry. The lowest-energy channel for levels with B_2 symmetry is located around 60.4 cm^{-1} above the lowest dissociation energy. Therefore, it is possible to have bound states of B_2 symmetry above the first dissociation threshold for $J = 0$.

Similarly to the $J = 0$ case, the lowest-lying accessible dissociation channels in the different $C_{2v}(M)$ symmetry manifolds can be derived for $J > 0$ states. For $J = 1$ states with A_1 symmetry, Table 1 shows that both j_1 and j_2 need to be even. Because of eq 1, $j_1 = j_2 = 2$ should hold for the lowest dissociation energy available for the $J = 1$ levels with A_1 symmetry, which lies approximately 181.2 cm^{-1} above the first dissociation threshold.

Table 2 summarizes the available dissociation channels for different J values classified according to the symmetry species of the $C_{2v}(M)$ symmetry group. As shown in Table 2, for all states with B_1 and B_2 symmetry, the lowest-energy dissociation channels have $j_1 = 1$. The lowest-energy dissociation channels for odd J states with A_1 and A_2 symmetry species have $j_1 = 2$ and $j_1 = 0$, respectively, while those for even J states with A_1 and A_2 symmetry species have $j_1 = 0$ and $j_1 = 2$, respectively. Because of this restriction for the lowest-energy channels available, bound states can exist up to around 181.2 cm^{-1} above $D_0 = 1775.42$ cm^{-1}.

Table 2. Dissociation Channels Categorized by Total Angular Momentum Quantum Number J and Symmetry Species (Symm.) of the $C_{2v}(M)$ Molecular Symmetry Group[a]

J	Symm.	(j_1, j_2)	$E_{diss} - D_0$
0	A_1	**(0,0)**, (2,2), (4,4), ⋯	0
0	B_2	**(1,1)**, (3,3), (5,5),⋯	60.4
1	A_1	**(2,2)**, (4,4), (6,6),⋯	181.2
1	A_2	**(0,1)**, (2,1), (2,3), (4,3), (4,5),⋯	0
1	B_1	**(1,0)**, (1,2), (3,2), (3,4),⋯	60.4
1	B_2	**(1,1)**, (3,3), (5,5),⋯	60.4
2	A_1	**(0,2)**, (2,0), (2,2), (2,4), (4,2),⋯	0
2	A_2	**(2,1)**, (2,3), (4,3), (4,5),⋯	181.2
2	B_1	**(1,2)**, (3,2), (3,4), (5,4),⋯	60.4
2	B_2	**(1,1)**, (1,3), (3,1), (3,3), (3,5),⋯	60.4
3	A_1	**(2,2)**, (2,4), (4,2), (4,4), (4,6),⋯	181.2
3	A_2	**(0,3)**, (2,1), (2,3), (2,5), (4,1),⋯	0
3	B_1	**(1,2)**, (1,4), (3,0), (3,2),⋯	60.4
3	B_2	**(1,3)**, (3,1), (3,3), (3,5), (5,3),⋯	60.4
4	A_1	**(0,4)**, (2,2), (2,4), (2,6), (4,0),⋯	0
4	A_2	**(2,3)**, (2,5), (4,1),⋯	181.2
4	B_1	**(1,4)**, (3,2), (3,4),⋯	60.4
4	B_2	**(1,3)**, (1,5), (3,1),⋯	60.4
⋮	⋮	⋮	⋮

[a]Dissociation channels are labeled as (j_1, j_2), where j_1 represents the rotational quantum number for the rotational motion of the H_2^+ moiety and j_2 represents the rotational quantum number for the rotational motion of the "pseudodiatomic" unit composed of He and the center of mass of H_2^+. The (j_1, j_2) channels having the lowest energy in the respective categories are given in bold, and their approximate energies measured from D_0 are given in the rightmost column using the formula $Bj_1(j_1 + 1)$ with $B = 30.2$ cm^{-1}.

3.2. Bound Rovibrational States. In previous theoretical studies, bound rovibrational states of H_2He^+ were determined to facilitate the detection of H_2He^+ in outer space,[9−11] as well as to investigate the role of bound states in the radiative

DOI: 10.1021/acs.jctc.7b01136
J. Chem. Theory Comput. 2018, 14, 1523−1533

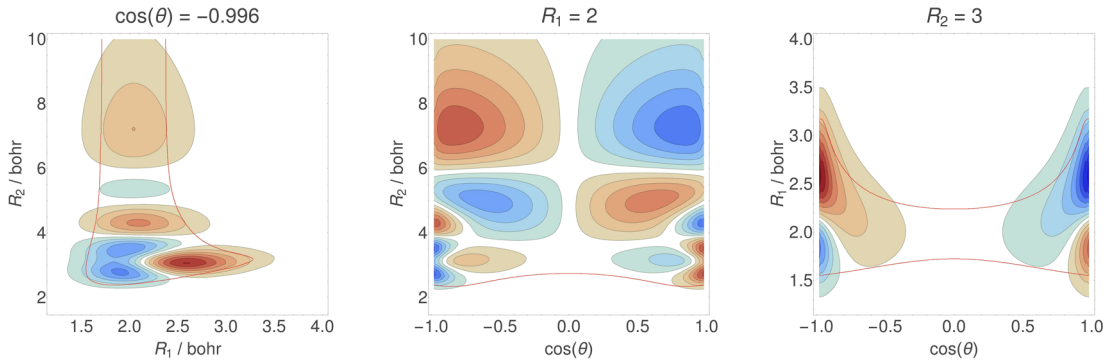

Figure 2. Nodal structure of the vibrational eigenstate of H_2He^+ located at 1809.0 cm^{-1} above its zero-point vibrational energy. The thin red line represents the border of the classically allowed region for this molecular vibration; i.e., along the red thin line the energy values of the PES equal the energy of the vibrational eigenstate.

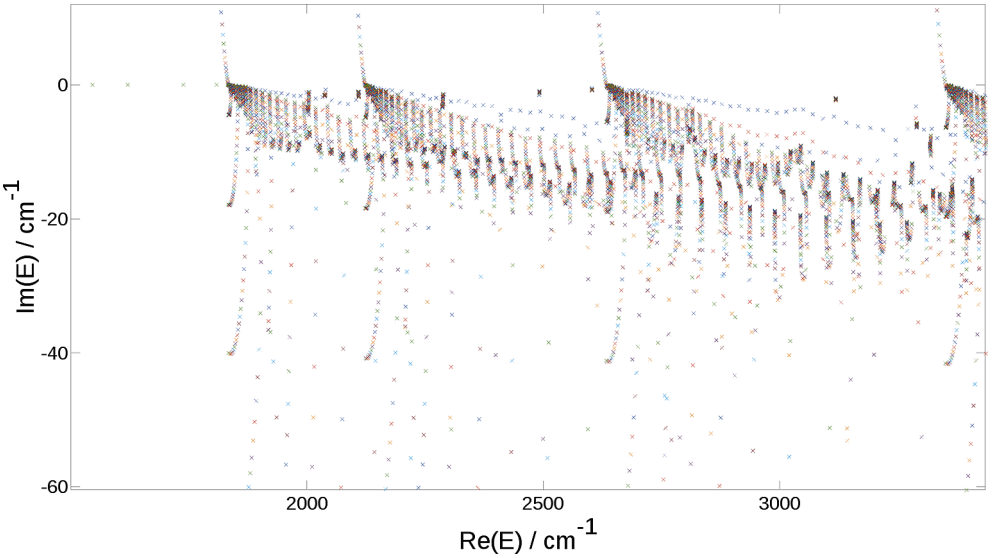

Figure 3. D^2FOPI-CCS eigenvalue trajectories of H_2He^+ on the complex energy plane, which are obtained by varying the scaling parameter of the complex coordinate scaling method between 0.02 and 0.80 in 40 steps.

association reactions producing H_2He^+.[11,14] Furthermore, rovibrational levels supported by the MRCI8 PES of ref 7 were computed and characterized by two of the present authors for elucidating the laser-induced alignment dynamics of H_2He^+.[36]

Next, we briefly summarize the characteristics of the bound states of H_2He^+ and emphasize features that have not been discussed in detail in the literature. The H_2He^+ molecular cation has a linear equilibrium structure, with a HeH distance that is shorter than the HH distance (Figure 1) and a first dissociation energy of D_0 = 1775 cm^{-1}.[7] In the low-energy region, the rotational and rovibrational levels correspond to a linear structure; however, when the energy increases, the simultaneous excitation along the R_2 stretching and the θ bending coordinates leads to the delocalization of He around the H_2^+ moiety.[36] The first vibrational state of H_2He^+ in which a nodal line appears perpendicular to the H−H bond is located 1809.0 cm^{-1} above the zero-point vibrational energy (ZPVE). This energy is lower than the vibrational fundamental of isolated H_2^+, 2191.1 cm^{-1}.[7] Thus, the attachment of He to H_2^+ results in the weakening of the H−H bond in H_2^+. It should be emphasized that the vibrationally excited state at 1809.0 cm^{-1}, having B_2 symmetry, lies above the first dissociation limit of the complex but below the second dissociation limit, which is the first available channel for states having J = 0 and B_2 symmetry. The nodal structure of the vibrational state located at 1809.0 cm^{-1} is shown in Figure 2. As seen in the leftmost panel, at shorter R_2 distances, where the perturbation effect of He is expected to be most prominent, a node appears along the R_1 coordinate, that is, along the H−H bond. In contrast, for longer R_2 distances the node dissapears, corresponding to the strengthening of the H−H bond. The drastic variation of the nodal structure reflects the strong nonlinear coupling between the motion along the R_1 and R_2 coordinates in the higher vibrational energy regions. This strong vibrational coupling was identified theoretically in the laser-induced photodissociation of H_2He^+[17] as well as in the reduced-dimensional computations of ref 14.

The MRCI8 PES of ref 7 supports 16 vibrational and about 420 rovibrational bound states below the first dissociation limit of H_2He^+.[36] However, as discussed in the previous section, bound rovibrational levels exist above the first and even the second dissociation limits. By taking these levels into account, the total number of bound rovibrational levels of H_2He^+ increases significantly, to around 520.

3.3. Resonance States of the H_2He^+ Complex. In previous studies, selected rovibrational resonance states of H_2He^+ were computed using the stabilization method.[12,14−16] In the present study, we computed resonances supported by the most accurate PES to date, MRCI8,[7] using three different

DOI: 10.1021/acs.jctc.7b01136
J. Chem. Theory Comput. 2018, 14, 1523−1533

techniques: CCS, CAP, and the stabilization method. The detailed discussion of our results follow this order.

Before examining the computed rovibrational resonances of H_2He^+ in detail, it is worth inspecting the CCS eigenvalue trajectories on the complex plane, which are generated during the D^{2}FOPI-CCS computations. The eigenvalue trajectories generated by the CCS method show (i) the appearance of dissociation channels, (ii) convergence of the computations, and (iii) the position of long-lived resonances in the complex energy plane.

Figure 3 depicts the D^{2}FOPI-CCS eigenvalue trajectories obtained for the $J = 0$ states with B_2 symmetry. As shown in Figure 3, the eigenvalue trajectories of the bound states having energies less than $D_1 \cong D_0 + 2B$ are localized and can only appear as single points. Out of the hundreds of trajectories shown in Figure 3, four can be seen to extend to the positive imaginary part of the complex plane. At first sight, these are numerical artifacts which do not carry physical information. However, the points where these trajectories cross the real axis represent the appearance of new dissociation channels, an observation which can be confirmed by the energy spacing of these crossing points. The separations correspond to those of the rovibrational transition energies of an isolated H_2^+ molecule. The appearance of new dissociation channels is also confirmed by the fact that rotated continua corresponding to different dissociation channels appear at the crossing points, which is a characteristic feature of CCS. Further important points in Figure 3 are as follows: (i) A large number of cusps in the eigenvalue trajectories are located between the imaginary energy values of around 10−20 cm^{-1}. (ii) Around a dozen of highly localized trajectories can be seen within a few cm^{-1} distance from the real energy axis, corresponding to resonances having much longer lifetimes than those in the imaginary energy region of 10−20 cm^{-1}. Hereafter, we refer to these longer-lived resonances as *isolated resonances*.

Tables 3 and 4 list the computed $J = 0$ vibrational and $J = 1$ rovibrational resonances of H_2He^+, respectively, obtained by the CCS method. The computed $J = 2$ rovibrational resonances are given in the Supporting Information. The resonances presented in Tables 3 and 4 are either isolated resonances or those appearing closely above a dissociation channel and having half-widths of $|\Gamma/2| < 1$ cm^{-1}, where $\hbar\Gamma^{-1}$ is the lifetime of the resonance state. All resonances in Table 3 were also obtained by the CAP method. It was found that the results obtained by the CAP method agree well with those obtained with the CCS method. Indeed, all resonance positions agree to within 0.1−1.6 cm^{-1}. Resonance lifetimes agree usually within a factor of 2, but they are always within the same order of magnitude. In Tables 3 and 4, the first resonances appearing above the respective dissociation channels are indicated with bold, while the resonances having energies larger than D_0 but smaller than their first allowed dissociation limit are indicated with italics.

As shown in Tables 3 and 4, the dissociation channels appearing in the numerical computations are consistent with the predictions of Section 2. Indeed, only even j_1 dissociation channels appear for states with A_1 and A_2 symmetry, while only odd j_1 dissociation channels appear for states with B_1 and B_2 symmetry. In addition, in the A_2 and B_1 symmetry manifolds of the $J = 1$ states, the dissociation channels appear as closely spaced pairs, corresponding to two different possible j_2 values for a given j_1 value.

The opening of dissociation channels can also be seen clearly in the stabilization histograms. The $J = 0$ vibrational stabilization histogram, generated using GENIUSH energies, is shown in Figure 4, whereby 16 spike-like peaks, corresponding to long-lived resonance states, can be identified in the energy region above D_0. Apart from the spike-like peaks at the energies of the bound states below the first B_2-symmetry dissociation channel, the energy spacings of the peaks above D_0 in the stabilization histogram coincide with those of the rovibrational transition energies of the H_2^+ molecule, which means that dissociation channels associated with the rotational and vibrational excitations in H_2^+ are opened.

Within a few tens of cm^{-1} above the opening of each dissociation channel, resonances appear, whose lifetimes reach several ps or several tens of ps and their wave functions are delocalized significantly along the R_2 coordinate.

Within the few tens of cm^{-1} energy range above a given dissociation channel opening, the lifetimes of these resonances decrease with the increase in energy and the number of nodes of their wave functions along the R_2 coordinate increases, indicating that the relative kinetic energy of the separating moieties in the dissociation process increases.

Table 3. Vibrational Resonances of H_2He^+ Having $J = 0$ and Their Characteristics[a]

J	Symm.	Re(E_{res})	Im(E_{res})	lifetime	Re(E_{res}) − D_0	(j_1, j_2)
0	A_1	**1775.9**	**> −0.01**	**>530.9**	**0.6**	(0,0)
0	A_1	1777.0	−0.13	20.4	1.7	
0	A_1	1779.8	−0.43	6.2	4.4	
0	A_1	1822.6	−0.06	43.5	47.3	
0	A_1	**1950.7**	**> −0.02**	**>132.7**	**175.4**	(2,2)
0	A_1	1951.8	−0.23	11.5	176.5	
0	A_1	2228.9	−4.52	0.6	453.6	
0	A_1	2321.1	−3.50	0.8	545.8	
0	A_1	**2352.0**	**> −0.22**	**>12.1**	**576.7**	(4,4)
0	A_1	2354.8	−0.38	7.0	579.5	
0	A_1	2930.3	−4.12	0.6	1155.0	
0	A_1	**2969.5**	**> −0.50**	**>5.3**	**1194.2**	(6,6)
0	B_2	*1809.0*	*0.00*	∞	*33.7*	
0	B_2	*1832.0*	*0.00*	∞	*56.7*	
0	B_2	**1834.2**	**−0.04**	**66.4**	**58.8**	(1,1)
0	B_2	1835.5	−0.13	20.4	60.2	
0	B_2	2002.0	−3.30	0.8	226.7	
0	B_2	2038.7	−1.51	1.8	263.4	
0	B_2	2109.4	−1.70	1.6	334.1	
0	B_2	**2123.6**	**−0.13**	**20.4**	**348.3**	(3,3)
0	B_2	2125.5	−0.22	12.3	350.1	
0	B_2	2286.4	−3.03	0.9	511.1	
0	B_2	2491.9	−0.91	2.9	716.6	
0	B_2	2602.9	−0.87	3.1	827.6	
0	B_2	**2635.1**	**−0.36**	**7.5**	**859.7**	(5,5)
0	B_2	2638.0	−0.45	5.9	862.7	
0	B_2	2642.2	−0.58	4.6	866.9	

[a]The first resonances appearing above the respective dissociation limits are printed bold. The dissociation channels are designated using (j_1, j_2) in the rightmost column, where j_1 represents the rotational quantum number for the rotational motion of the H_2^+ moiety and j_2 represents the rotational quantum number for the rotational motion of the "pseudodiatomic" unit composed of He and the center of mass of H_2^+. The energies of the resonances whose energies are larger than D_0 but smaller than their respective symmetrically allowed first dissociation limits are labeled in italics. The real part and the imaginary part of the resonance eigenvalues are denoted as Re(E_{res}) and Im(E_{res}), respectively, and are given in cm^{-1}. Lifetimes are given in picoseconds. Symmetry designations correspond to the C_{2v}(M) molecular symmetry group.

DOI: 10.1021/acs.jctc.7b01136
J. Chem. Theory Comput. 2018, 14, 1523−1533

Table 4. Rovibrational Resonances of H_2He^+ Having $J = 1$ and Their Characteristics[a]

J	Symm.	Re(E_{res})	Im(E_{res})	lifetime	Re(E_{res}) − D_0	(j_1, j_2)
1	A_1	*1817.8*	*0.00*	∞	*42.5*	
1	A_1	*1911.8*	*0.00*	∞	*136.5*	
1	A_1	*1941.3*	*0.00*	∞	*166.0*	
1	A_1	**1950.8**	**−0.19**	**14.0**	**175.5**	(2,2)
1	A_1	1953.7	−0.66	4.0	178.4	
1	A_1	2168.4	−1.78	1.5	393.1	
1	A_1	2296.5	−0.43	6.2	521.2	
1	A_1	**2353.2**	**−0.52**	**5.1**	**577.9**	(4,4)
1	A_1	2354.4	−0.45	6.0	579.1	
1	A_1	2410.5	−1.27	2.1	635.2	
1	A_1	2698.8	−1.68	1.6	923.5	
1	A_1	2878.6	−1.78	1.5	1103.3	
1	A_1	2966.0	−0.84	3.2	1190.7	
1	A_1	**2971.6**	**−1.52**	**1.7**	**1196.3**	(6,6)
1	A_2	**1776.5**	**> −0.17**	**>15.6**	**1.2**	(0,1)
1	A_2	1816.5	−0.03	88.5	41.2	
1	A_2	1828.4	−0.13	19.7	53.1	
1	A_2	1911.8	−0.09	30.7	136.5	
1	A_2	1940.8	−0.24	11.1	165.5	
1	A_2	1945.6	−3.25	0.8	170.3	
1	A_2	**1950.5**	**> −0.13**	**>20.4**	**175.2**	(2,1 or 3)
1	A_2	**1951.4**	**> −0.37**	**>7.2**	**176.1**	(2,1 or 3)
1	A_2	1953.0	−0.25	10.4	177.7	
1	A_2	2166.0	−2.46	1.1	390.7	
1	A_2	2234.2	−3.41	0.8	458.9	
1	A_2	2292.5	−2.84	0.9	517.2	
1	A_2	2326.3	−2.64	1.0	551.0	
1	A_2	2351.3	−2.11	1.3	576.0	
1	A_2	**2353**	**−0.47**	**5.7**	**577.7**	(4,3 or 5)
1	A_2	**2354.5**	**−0.96**	**2.8**	**579.2**	(4,3 or 5)
1	A_2	2357.1	−0.44	6.0	581.8	
1	A_2	2698.8	−5.72	0.5	923.5	
1	A_2	2794.7	−8.38	0.3	1019.4	
1	A_2	2879.7	−5.41	0.5	1104.4	
1	A_2	2931.3	−3.16	0.8	1156.0	
1	A_2	2967.2	−2.44	1.1	1191.9	
1	A_2	**2970.7**	**> −0.94**	**>2.8**	**1195.4**	(6,5 or 7)
1	A_2	**2972.7**	**> −1.93**	**>1.4**	**1197.4**	(6,5 or 7)
1	B_1	*1812.0*	*0.00*	∞	*36.7*	
1	B_1	*1819.6*	*0.00*	∞	*44.3*	
1	B_1	**1833.8**	**> −0.01**	**>379.2**	**58.5**	(1,0 or 2)
1	B_1	**1834.6**	**−0.12**	**21.4**	**59.3**	(1,0 or 2)
1	B_1	1834.9	−0.14	19.0	59.6	
1	B_1	1837.6	−0.72	3.7	62.3	
1	B_1	1961.1	−0.48	5.6	185.8	
1	B_1	2009.0	−3.35	0.8	233.7	
1	B_1	2040.9	−2.84	0.9	265.6	
1	B_1	2077.8	−0.17	15.5	302.5	
1	B_1	2110.3	−1.69	1.6	335.0	
1	B_1	**2123.7**	**> −0.17**	**>15.6**	**348.4**	(3,2 or 4)
1	B_1	**2124.7**	**> −0.53**	**>5.0**	**349.4**	(3,2 or 4)

DOI: 10.1021/acs.jctc.7b01136
J. Chem. Theory Comput. 2018, 14, 1523−1533

Table 4. continued

J	Symm.	Re(E_{res})	Im(E_{res})	lifetime	Re(E_{res}) − D_0	(j_1, j_2)
1	B_1	2125.4	−0.37	7.1	350.1	
1	B_1	2292.9	−4.13	0.6	517.6	
1	B_1	2421.2	−2.06	1.3	645.9	
1	B_1	2497.7	−2.37	1.1	722.4	
1	B_1	2568.5	−1.36	2.0	793.2	
1	B_1	2606.1	−1.46	1.8	830.8	
1	B_1	**2635.4**	**−0.37**	**7.2**	**860.1**	(5,4 or 6)
1	B_1	2635.5	−0.40	6.6	860.2	
1	B_1	**2637.7**	**> −1.43**	**>1.9**	**862.4**	(5,4 or 6)
1	B_2	*1819.1*	*0.00*	∞	*43.8*	
1	B_2	**1834.5**	**> −0.10**	**>27.7**	**59.2**	(1,1)
1	B_2	1837.4	−0.72	3.7	62.1	
1	B_2	1962.3	−0.40	6.6	187.0	
1	B_2	2076.3	−0.001	1986.7	301.0	
1	B_2	**2124.0**	**> −0.25**	**>10.6**	**348.7**	(3,3)
1	B_2	2125.5	−0.34	7.9	350.2	
1	B_2	2422.2	−2.03	1.3	646.9	
1	B_2	2569.9	−1.95	1.4	794.6	
1	B_2	**2637.0**	**−0.71**	**3.7**	**861.7**	(5,5)
1	B_2	2637.1	−0.91	2.9	861.8	

[a]The first resonances appearing above the respective dissociation limits are printed bold. The dissociation channels are designated using (j_1, j_2) in the rightmost column, where j_1 represents the rotational quantum number for the rotational motion of the H_2^+ moiety and j_2 represents the rotational quantum number for the rotational motion of the "pseudodiatomic" unit composed of He and the center of mass of H_2^+. The energies of the resonances whose energies are larger than D_0 but smaller than their simmetrically allowed first dissociation limits are labeled in italics. The real part and the imaginary part of the resonance eigenvalues are denoted as Re(E_{res}) and Im(E_{res}), respectively, and are given in cm^{-1}. Lifetimes are given in picoseconds. Symmetry designations correspond to the C_{2v}(M) molecular symmetry group.

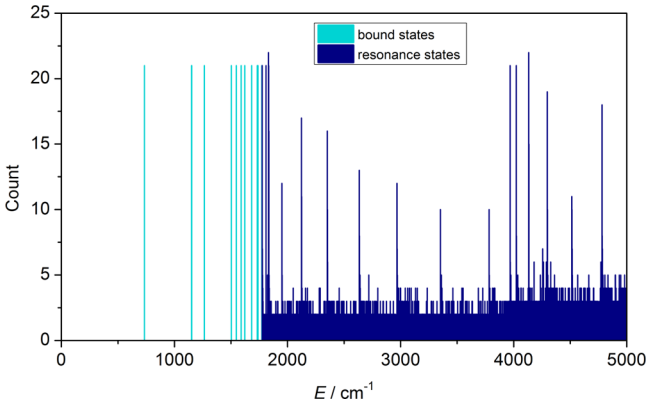

Figure 4. Stabilization histogram of H_2He^+ based on 21 number of GENIUSH computations with $R_{2,max}$/bohr ∈ [49.0,51.0] (see Supporting Information for details). A bin size of 0.05 cm^{-1} has been adopted to generate this figure.

3.3.1. Properties of Long-Lived and Isolated Resonances. Figure 5 shows two-dimensional probability density plots of the J = 0 A_1-symmetry resonance located at 1822.6 cm^{-1}, having a lifetime of 43.5 ps. The nodal structure of the plots shows clearly that this is a Feshbach-type resonance,[19] in which the surplus energy, that above the dissociation limit, is distributed in the motion along the nondissociative coordinates R_1 and θ. The upper leftmost panel of Figure 5 shows a node along R_1 at around R_2 = 3 bohr, while the upper middle panel of Figure 5 shows that j_1 = 2 should be assigned to this resonance. Considering that only the j_1 = j_2 = 0 dissociation channel is open energetically, not only vibrational predissociation but also rotational predissociation can proceed via this resonance.

Figure 6 shows two-dimensional probability density plots of the J = 0, B_2-symmetry resonance located at 2286.4 cm^{-1}, having a lifetime of 0.9 ps. Two dissociation channels of j_1 = 1 and j_1 = 3 are opened energetically at this resonance. The upper middle panel of Figure 6 shows that j_1 = 3 can be assigned to this resonance at around R_2 = 3 bohr and j_1 = 5 can be assigned to this resonance at around R_2 = 5 bohr. Comparison of the upper leftmost and lower leftmost panels reveals prominent coupling between R_1 and θ, which can also be seen in the upper rightmost panel. A further important aspect of Figure 6 is that an alternating nodal structure appears in the region above R_2 = 6 bohr along the R_2 coordinate in the lower middle panel, which can be regarded as a pattern originating from an interference between the j_1 = 1 and the j_1 = 3 dissociation channels. This interference between the dissociation channels is discussed further in the next section.

3.3.2. Dissociation Branching Ratios. Next, we discuss a useful computational technique for obtaining both qualitative and quantitative information about the computed rovibrational resonance states of H_2He^+. By taking advantage of the versatile nature of the GENIUSH program suite, it is straightforward to implement a reduced-dimensional model of H_2He^+, whereby the intermonomer distance R_2 is kept fixed at a large value of 80 bohr. In this reduced-dimensional model the interactions between H_2^+ and He can be neglected; therefore, we can obtain the eigenstates of the free H_2^+ molecular cation. Assigning vibrational and rotational quantum numbers to these states is straightforward.

DOI: 10.1021/acs.jctc.7b01136
J. Chem. Theory Comput. 2018, 14, 1523−1533

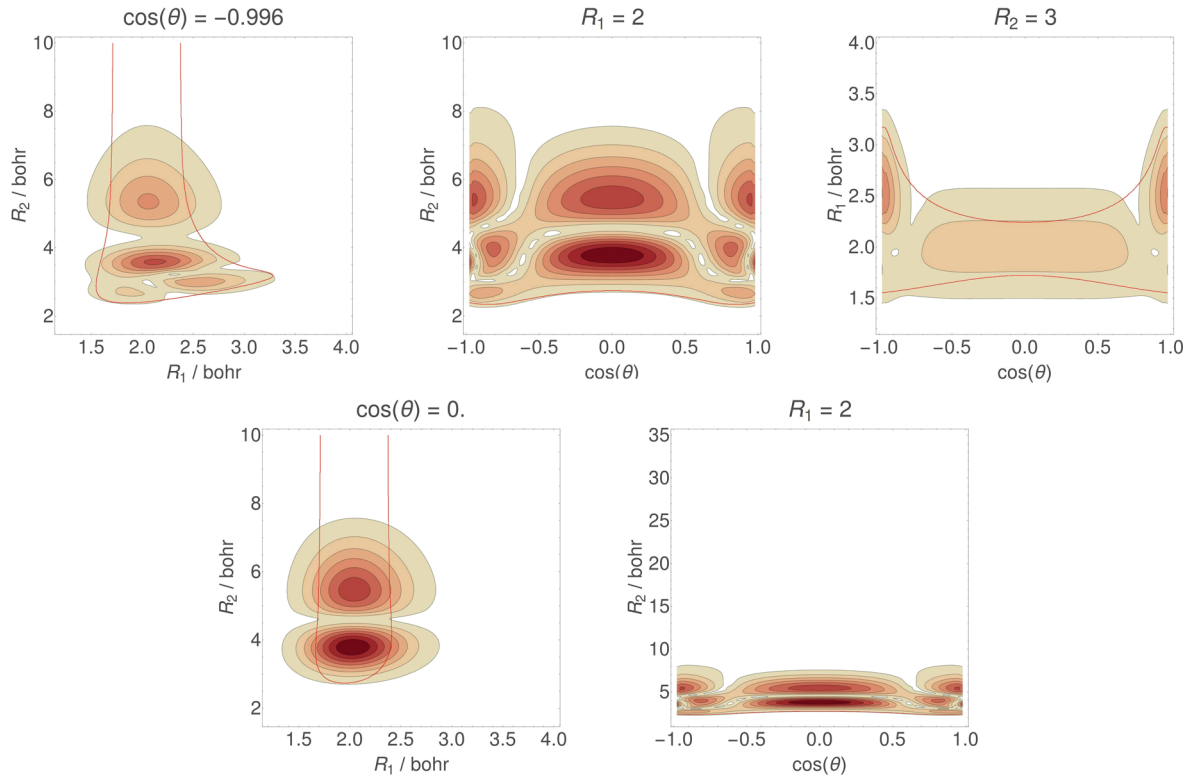

Figure 5. Nodal structures of the $J = 0$ vibrational resonance of H_2He^+ located at around 1822.6 cm^{-1} above its ZPVE. The lifetime of this resonance is 43.5 ps. The thin red line represents the border of the classically allowed region of the molecular vibration.

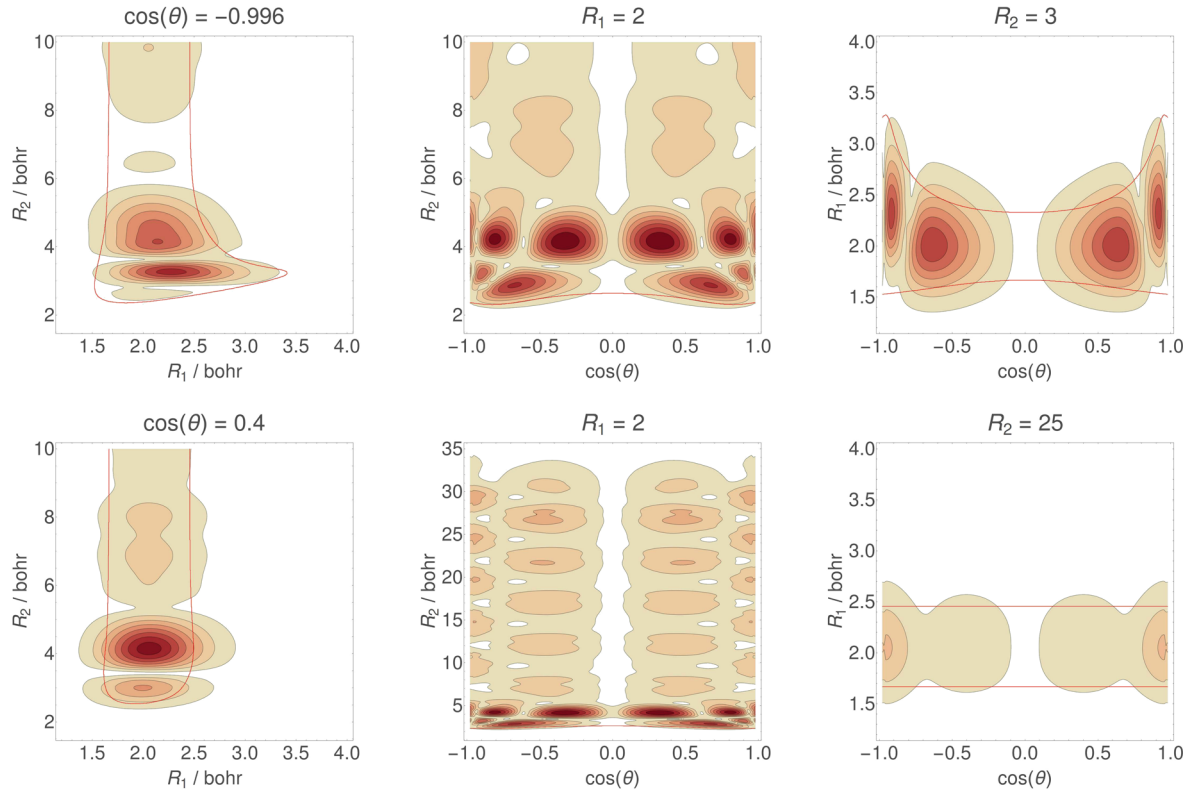

Figure 6. Nodal structures of the $J = 0$ vibrational resonance of H_2He^+ located at 2286.4 cm^{-1} above its ZPVE. The lifetime of this resonance is 0.9 ps. The thin red line represents the border of the classically allowed region of the molecular vibration.

Since in the reduced-dimensional computation we can use the same direct-product DVR basis that was used in the full-dimensional computations, it is possible to project the full-dimensional wave functions onto the reduced-dimensional

DOI: 10.1021/acs.jctc.7b01136
J. Chem. Theory Comput. 2018, 14, 1523−1533

Table 5. Overlap Values between 17 Selected Resonances Obtained by Full-Dimensional Calculations and Eigenstates Obtained by Reduced-Dimensional Calculations Where R_2 Is Fixed at 80 bohr[a]

		$(v_{H_2^+}j_1)$									
Re(E_{res})	R_2	(0,0)	(0,1)	(0,2)	(0,3)	(0,4)	(0,5)	(0,8)	(1,0)	(1,1)	(1,2)
1775.9[b]	32	**1.00**	0.00	0.00	0.00	0.00	0.00	0.00	0.00	0.00	0.00
1834.2[b]	34	0.00	**1.00**	0.00	0.00	0.00	0.00	0.00	0.00	0.00	0.00
1950.7[b]	34	0.00	0.00	**1.00**	0.00	0.00	0.00	0.00	0.00	0.00	0.00
2123.6[b]	36	0.00	0.00	0.00	**1.00**	0.00	0.00	0.00	0.00	0.00	0.00
2352.0[b]	36	0.00	0.00	0.00	0.00	**1.00**	0.00	0.00	0.00	0.00	0.00
2635.1[b]	36	0.00	0.00	0.00	0.00	0.00	**1.00**	0.00	0.00	0.00	0.00
2038.7	6	0.00	0.04	0.00	**0.96**	0.00	0.00	0.00	0.00	0.00	0.00
	29	0.00	**1.00**	0.00	0.00	0.00	0.00	0.00	0.00	0.00	0.00
2109.4	7	0.00	0.04	0.00	**0.96**	0.00	0.00	0.00	0.00	0.00	0.00
	29	0.00	**1.00**	0.00	0.00	0.00	0.00	0.00	0.00	0.00	0.00
2228.9	5	0.04	0.00	0.04	0.00	**0.92**	0.00	0.00	0.00	0.00	0.00
	29	**0.89**	0.00	0.11	0.00	0.00	0.00	0.00	0.00	0.00	0.00
2286.4	5	0.00	0.03	0.00	0.06	0.00	**0.91**	0.00	0.00	0.00	0.00
	29	0.00	**0.22**	0.00	**0.78**	0.00	0.00	0.00	0.00	0.00	0.00
2321.1	7	0.07	0.00	0.02	0.00	**0.91**	0.00	0.00	0.00	0.00	0.00
	29	**0.74**	0.00	**0.26**	0.00	0.00	0.00	0.00	0.00	0.00	0.00
2491.9	5	0.00	0.01	0.00	0.02	0.00	**0.97**	0.00	0.00	0.00	0.00
	29	0.00	**0.86**	0.00	0.14	0.00	0.00	0.00	0.00	0.00	0.00
2602.9	7	0.00	0.01	0.00	0.00	0.00	**0.99**	0.00	0.00	0.00	0.00
	29	0.00	**0.96**	0.00	0.04	0.00	0.00	0.00	0.00	0.00	0.00
3963.6[c]	8	0.00	0.00	0.00	0.00	0.00	0.00	0.01	**0.99**	0.00	0.00
	39	0.00	0.00	0.00	0.00	0.01	0.00	**0.99**	0.00	0.00	0.00
3968.2[b,c]	39	0.00	0.00	0.00	0.00	0.00	0.00	0.00	**1.00**	0.00	0.00
4023.5[b,c]	39	0.00	0.00	0.00	0.00	0.00	0.00	0.00	0.00	**1.00**	0.00
4124.4[c]	8	0.13	0.00	0.00	0.00	**0.43**	0.00	0.07	0.07	0.00	**0.30**
	39	0.00	0.00	0.01	0.00	0.04	0.00	**0.43**	**0.52**	0.00	0.00

[a]Overlaps were computed by fixing R_2 at given values in the full-dimensional wave functions. The vibrational quantum number $v_{H_2^+}$ and the rotational quantum number j_1 of the H_2^+ moiety are assigned to the respective resonances based on reduced-dimensional calculations. Resonance positions are given in cm^{-1}, R_2 values are in bohr. The overlap values are calculated using GENIUSH-CAP, while the resonance positions are those computed by D^2FOPI-CCS, to be consistent with Table 3. [b]These states appear as the first resonances above a specific dissociation channel opening. [c]The lifetimes of the resonances at 3963.6, 3968.2, 4023.5, and 4124.4 cm^{-1} are 2.1, 49, 0.5, and 29 ps, respectively.

ones. This approach to the assignment of approximate quantum numbers to rovibrational resonance states has similarity to the so-called *rigid-rotor decomposition* (RRD) scheme[37] and can be considered as a simplified version of the *coupled-rotor decomposition* (CRD)[38] scheme, a sophisticated and widely applicable method for determining symmetry and approximate quantum number information for rovibrational states of dimers.

By calculating the overlaps between the full-dimensional wave functions at a large R_2 distance in the asymptotic region and the reduced-dimensional wave functions, we can assign quantum numbers to the dissociation products and derive dissociation probabilities of a given resonance into the different dissociation channels, yielding dissociation branching ratios. By computing overlaps at a given R_2 value at the interaction region and by comparing them with those obtained at a given R_2 value in the asymptotic region, one can judge whether a resonance is of Feshbach type. Overlaps computed for some resonances are presented in Table 5, a few selected examples are discussed below.

All the overlaps between the $J = 0$, B_2-symmetry resonance state located at 2109.4 cm^{-1} and the reduced-dimensonal eigenstates at $R_2 = 29$ bohr give values close to zero, except for one reduced-dimensional level, having $v_{H_2^+} = 0$ and $j_1 = 1$. Therefore, the resonance state located at 2109.4 cm^{-1} decays solely to He + H_2^+, whereby H_2^+ is in the first rotationally excited state of the vibrational ground state. On the other hand, the overlaps at $R_2 = 7$ bohr give the assignment of $(v_{H_2^+}, j_1) = (0, 3)$, which indicates rotational predissociation.

For the $J = 0$, B_2-symmetry resonance at 2286.4 cm^{-1}, for which an interference pattern between different dissociation channels can be recognized at large R_2 values in Figure 6, there are two reduced-dimensional eigenstates showing significant overlaps with the full-dimensional wave function at $R_2 = 29$ bohr. The $(v_{H_2^+}, j_1) = (0, 1)$ state of H_2^+ gives a contribution of 22%, while the $(v_{H_2^+}, j_1) = (0, 3)$ state gives a contribution of 78%. Therefore, one can conclude that the resonance state at 2286.4 cm^{-1} dissociates into He + $H_2^+(j_1 = 1)$ with 22% probability and into He + $H_2^+(j_1 = 3)$ with 78% probability.

In the asymptotic region, for all of the resonances that appear just above the threshold for the respective dissociation channels, only one significant overlap can be found, corresponding to the respective dissociation channel. These resonances have diffuse wave functions with very small amplitudes in the interaction region. Therefore, their overlaps computed with the reduced-dimensional eigenstates in the interaction region have large numerical errors and are therefore not presented.

A few resonances having the energies almost as high as or higher than the first dissociation channel corresponding to $v_{H_2^+} = 1$ are also shown in Table 5. The resonance at 3963.6 cm^{-1} shows pure vibrational excitation in H_2^+, that is, $(v_{H_2^+}j_1) = (1,0)$ in the interaction region, while it shows $(v_{H_2^+}j_1) = (0,8)$ in the

DOI: 10.1021/acs.jctc.7b01136
J. Chem. Theory Comput. 2018, 14, 1523−1533

asymptotic region. This indicates that there is significant energy transfer from the vibration of H_2^+ into the rotation of H_2^+ during the dissociation process. This observation can be used to rationalize the long, 2.1 ps lifetime of this resonance state. As shown in the bottom two rows of Table 5, the resonance at 4124.4 cm^{-1} exhibits a strong mixing of the rovibrational eigenstates of H_2^+; i.e., in the interaction region the contributions of $(v_{H_2^+}, j_1)$ = (0,0), (0,4), (0,8), (1,0), and (1,2) are 13%, 43%, 7%, 7%, and 30%, respectively, while in the asymptotic region the contributions are changed to 0%, 4%, 43%, 52%, and 0%, in order. This shows that during the course of the dissociation both rotational excitation of H_2^+ in the $v_{H_2^+}$ = 0 manifold and rotational deexcitation of H_2^+ in the $v_{H_2^+}$ = 1 manifold proceeds. It can be concluded that the interference between dissociation channels of different $v_{H_2^+}$ vibrational manifolds can lead to the important phenomenon that for some specific $v_{H_2^+}$ values the rotational excitation of H_2^+ occurs during dissociation.

4. SUMMARY AND CONCLUSIONS

Rovibrational resonance states of H_2He^+ have been determined and characterized in the present study. On the basis of symmetry considerations and angular momentum couplings, the possible dissociation channels of this complex have been classified. By using an accurate PES called MRCI8,[7] the energies and wave functions of the bound and resonance rovibrational levels of H_2He^+ have been obtained numerically by complex coordinate scaling, complex absorbing potential, and stabilization techniques.

It was found that nearly 20% of the bound rovibrational levels of H_2He^+ are located above D_0. By investigating rovibrational levels with J = 0, J = 1, and J = 2, as many as around 200 long-lived rovibrational resonances of H_2He^+ have been characterized in the energy region of $[D_0, D_0 + 3000]$ cm^{-1}. Anharmonic vibrational mode couplings, rotation−vibration interactions, and mechanisms of the stabilization of resonance states have been examined. The resonances at 1822.6 and 2286.4 cm^{-1} exhibit, for example, strong coupling between the vibration along the radial R_1 coordinate and the internal rotation of the H_2^+ moiety along the θ coordinate. Dissociation of resonances can proceed either as rotational predissociation, see Figures 5 and 6 for example, or as vibrational predissociation, see the resonance at 1822.6 cm^{-1}. An important finding of the present study is that in the asymptotic region the nodal structure of the wave functions of the resonances may exhibit interference patterns originating from coexisting dissociation channels.

Reduced-dimensional computations, in which R_2 is fixed at a large value, e.g., 80 bohr, have also been performed, and the overlaps between the wave functions obtained by this reduced-dimensional model and those obtained by the full-dimensional computations have been computed. These overlap values allow the assignment of rotational and vibrational quantum numbers to the resonances and the calculation of the branching ratios of the dissociation channels. The resulting branching ratios are consistent with the nodal structure of the wave functions appearing in the probability density plots. The analysis technique employed in this work should be highly useful for other molecular systems as well.

The accurate numerical results of this study, complemented with considerable physical insight, should prove to be useful for future investigations related to the molecular cation H_2He^+. The tools developed should also be useful during studies aimed at the fundamental understanding of similar weakly bound complexes.

In the only spectroscopic experiment[13] carried out on H_2He^+ ions so far, highly excited rovibrational levels, lying within a few cm^{-1} of the dissociation asymptote, were studied. In order to complement this work, future investigations might aim to study cold samples. A possible approach would be to use cryogenic ion traps[39−41] and to attach He atoms as done for the H_3^+·He system.[42] The resonance and bound states of H_2He^+ may then be detected by single- or multiphoton dissociation. We hope that the rovibrational transitions which can be deduced from the accurate rovibrational energies computed in the present study will considerably facilitate the detection of H_2He^+ in future spectroscopic measurements and eventually in outer space.

■ ASSOCIATED CONTENT

Supporting Information

The Supporting Information is available free of charge on the ACS Publications website at DOI: 10.1021/acs.jctc.7b01136.

Theoretical and computational details omitted from the manuscript. Table S1: computed bound rovibrational states of H_2He^+. Table S2: computed rovibrational resonances of H_2He^+ having J = 2. (PDF)

■ AUTHOR INFORMATION

Corresponding Author

*E-mail: tamas821@caesar.elte.hu.

ORCID

Tamás Szidarovszky: 0000-0003-0878-5212

Notes

The authors declare no competing financial interest.

■ ACKNOWLEDGMENTS

The authors are grateful to NKFIH for continued support (Grant No. PD124623 and No. K119658) and to MEXT for its support of JSPS KAKENHI (Grant No. JP15H05696).

■ REFERENCES

(1) Abel, T.; Anninos, P.; Zhang, Y.; Norman, M. L. Modeling primordial gas in numerical cosmology. *New Astron.* **1997**, *2*, 181−207.

(2) Coppola, C. M.; Longo, S.; Capitelli, M.; Palla, F.; Galli, D. Vibrational level population of H_2 and H_2^+ in the early universe. *Astrophys. J., Suppl. Ser.* **2011**, *193*, 7.

(3) Johnsen, R.; Chen, A.; Biondi, M. A. Dissociative charge transfer of He^+ ions with H_2 and D_2 molecules from 78 to 330 K. *J. Chem. Phys.* **1980**, *72*, 3085−3088.

(4) Jones, E. G.; Wu, L. C.; Hughes, B. M.; Tiernan, T. O.; Hopper, D. G. Collisional studies of the excited state potential energy surfaces of HeH_2^+: Energy thresholds and cross sections for reactions of helium ions with hydrogen yielding H^+, H_2^+, H_3^+, HeH^+, and H*(*nl*). *J. Chem. Phys.* **1980**, *73*, 5631−5645.

(5) Pollard, J. E.; Syage, J. A.; Johnson, L. K.; Cohen, R. B. Collinear reactive scattering of state−selected H_2^++He→HeH^++H: A method for probing dynamical resonances. *J. Chem. Phys.* **1991**, *94*, 8615−8617.

(6) Palmieri, P.; Puzzarini, C.; Aquilanti, V.; Capecchi, G.; Cavalli, S.; De Fazio, D.; Aguilar, A.; Gimenez, X.; Lucas, J. M. Ab initio dynamics of the He+H_2^+→HeH^++H reaction: a new potential energy surface and quantum mechanical cross-sections. *Mol. Phys.* **2000**, *98*, 1835−1849.

(7) De Fazio, D.; De Castro-Vitores, M.; Aguado, A.; Aquilanti, V.; Cavalli, S. The He+H_2^+ →HeH^++H reaction: Ab initio studies of the potential energy surface, benchmark time-independent quantum

DOI: 10.1021/acs.jctc.7b01136
J. Chem. Theory Comput. 2018, 14, 1523−1533

dynamics in an extended energy range and comparison with experiments. *J. Chem. Phys.* **2012**, *137*, 244306.
(8) Vera, M. H.; Schiller, S.; Wester, R.; Gianturco, A. Rotationally inelastic cross sections, rates and cooling times for *para*-H_2^+, *ortho*-D_2^+ and HD^+ in cold helium gas. *Eur. Phys. J. D* **2017**, *71*, 106.
(9) Tennyson, J.; Miller, S. Predicted vibration-rotation levels of H_2He^+ and its isotopomers. *J. Chem. Phys.* **1987**, *87*, 6648−6652.
(10) Juřek, M.; Špirko, V.; Kraemer, W. P. Ab initio calculated rotation-vibration linestrengths for HeH_2^+. *J. Mol. Spectrosc.* **1997**, *182*, 364−370.
(11) Šindelka, M.; Špirko, V.; Kraemer, W. P. Vibrational linestrengths for the ground and first excited electronic states of HeH_2^+. *Theor. Chem. Acc.* **2003**, *110*, 170−175.
(12) Kraemer, W. P.; Špirko, V.; Bludský, O. Bound and low-lying quasi-bound rotation-vibration energy levels of the ground and first excited electronic states of HeH_2^+. *Chem. Phys.* **2002**, *276*, 225−242.
(13) Carrington, A.; Gammie, D. I.; Shaw, A. M.; Taylor, S. M.; Hutson, J. M. Observation of a microwave spectrum of the long-range $He\cdots H_2^+$ complex. *Chem. Phys. Lett.* **1996**, *260*, 395−405.
(14) Mrugała, F.; Špirko, V.; Kraemer, W. P. Radiative association of HeH_2^+. *J. Chem. Phys.* **2003**, *118*, 10547−10560.
(15) Mrugała, F.; Kraemer, W. P. Radiative association of He^+ with H_2 at temperatures below 100 K. *J. Chem. Phys.* **2005**, *122*, 224321.
(16) Mrugała, F.; Kraemer, W. P. Radiative charge transfer in $He^+ + H_2$ collisions in the milli- to nano-electron-volt range: A theoretical study within state-to-state and optical potential approaches. *J. Chem. Phys.* **2013**, *138*, 104315.
(17) Szidarovszky, T.; Yamanouchi, K. Photodissociation dynamics of weakly bound HeH_2^+ in intense light fields. *Phys. Rev. A: At., Mol., Opt. Phys.* **2016**, *94*, 063405.
(18) Szidarovszky, T.; Császár, A. G.; Czakó, G. On the efficiency of treating singularities in triatomic variational vibrational computations. The vibrational states of H_3^+ up to dissociation. *Phys. Chem. Chem. Phys.* **2010**, *12*, 8373−8386.
(19) Moiseyev, N. *Non-Hermitian Quantum Mechanics*; Cambridge University Press, 2011.
(20) Szidarovszky, T.; Császár, A. G. Low-lying quasibound rovibrational states of $H_2{}^{16}O$. *Mol. Phys.* **2013**, *111*, 2131−2146.
(21) Mátyus, E.; Czakó, G.; Császár, A. G. Toward black-box-type full- and reduced-dimensional variational (ro)vibrational computations. *J. Chem. Phys.* **2009**, *130*, 134112.
(22) Fábri, C.; Mátyus, E.; Császár, A. G. Rotating full- and reduced-dimensional quantum chemical models of molecules. *J. Chem. Phys.* **2011**, *134*, 074105.
(23) Papp, D.; Szidarovszky, T.; Császár, A. G. A general variational approach for computing rovibrational resonances of polyatomic molecules. Application to the weakly bound H_2He^+ and H_2CO systems. *J. Chem. Phys.* **2017**, *147*, 094106.
(24) Papp, D.; Sarka, J.; Szidarovszky, T.; Császár, A. G.; Mátyus, E.; Hochlaf, M.; Stoecklin, T. Complex rovibrational dynamics of the $Ar{\cdot}NO^+$ complex. *Phys. Chem. Chem. Phys.* **2017**, *19*, 8152−8160.
(25) Light, J. C.; Carrington, T. Discrete-variable representations and their utilization. *Adv. Chem. Phys.* **2007**, *114*, 263−310.
(26) Moiseyev, N.; Friedland, S.; Certain, P. R. Cusps, θ trajectories, and the complex virial theorem. *J. Chem. Phys.* **1981**, *74*, 4739−4740.
(27) Jacobi, C. G. J. Sur l'élimination des noeuds dans le probléme des trois corps. *C. R. Hebd. Seances Acad. Sci.* **1842**, *15*, 236−255.
(28) Riss, U. V.; Meyer, H. D. Calculation of resonance energies and widths using the complex absorbing potential method. *J. Phys. B: At., Mol. Opt. Phys.* **1993**, *26*, 4503−4535.
(29) Muga, J. G.; Palao, J. P.; Navarro, B.; Egusquiza, I. L. Complex absorbing potentials. *Phys. Rep.* **2004**, *395*, 357−426.
(30) Mussa, H. Y.; Tennyson, J. Calculating quasi-bound rotation-vibrational states of HOCl using massively parallel computers. *Chem. Phys. Lett.* **2002**, *366*, 449−457.
(31) Skokov, S.; Bowman, J. M.; Mandelshtam, V. A. Calculation of resonance states of non-rotating HOCl using an accurate ab initio potential. *Phys. Chem. Chem. Phys.* **1999**, *1*, 1279−1282.
(32) Mandelshtam, V. A.; Ravuri, T. R.; Taylor, H. S. Calculation of the density of resonance states using tha stabilization method. *Phys. Rev. Lett.* **1993**, *70*, 1932−1935.
(33) Hazi, A. U.; Taylor, H. S. Stabilization method of calculating resonance energies: model problem. *Phys. Rev. A: At., Mol., Opt. Phys.* **1970**, *1*, 1109−1120.
(34) Bunker, P. R.; Jensen, P. *Molecular Symmetry and Spectroscopy*; NRC Research Press, 1998.
(35) Herzberg, G.; Jungen, C. Rydberg series and ionization potential of the H_2 molecule. *J. Mol. Spectrosc.* **1972**, *41*, 425−486.
(36) Szidarovszky, T.; Yamanouchi, K. Full-dimensional simulation of the laser-induced alignment dynamics of H_2He^+. *Mol. Phys.* **2017**, *115*, 1916−1926.
(37) Mátyus, E.; Fábri, C.; Szidarovszky, T.; Czakó, G.; Allen, W. D.; Császár, A. G. Assigning quantum labels to variationally computed rotational-vibrational eigenstates of polyatomic molecules. *J. Chem. Phys.* **2010**, *133*, 034113.
(38) Sarka, J.; Mátyus, E.; Császár, A. G. Rovibrational quantum dynamical computations for deuterated isotopologues of the methane-water dimer. *Phys. Chem. Chem. Phys.* **2017**, *19*, 15335−15345.
(39) Asvany, O.; Brunken, S.; Kluge, L.; Schlemmer, S. COLTRAP: a 22-pole ion trapping machine for spectroscopy at 4 K. *Appl. Phys. B: Lasers Opt.* **2014**, *114*, 203−211.
(40) Günther, A.; Nieto, P.; Müller, D.; Sheldrick, A.; Gerlich, D.; Dopfer, O. BerlinTrap: A new cryogenic 22-pole ion trap spectrometer. *J. Mol. Spectrosc.* **2017**, *332*, 8−15.
(41) Jasik, J.; Zabka, J.; Roithova, J.; Gerlich, D. Infrared spectroscopy of trapped molecular dications below 4 K. *Int. J. Mass Spectrom.* **2013**, *354*−*355*, 204−210.
(42) Savic, I.; Gerlich, D.; Asvany, O.; Jusko, P.; Schlemmer, S. Controlled synthesis and analysis of $He\text{-}H_3^+$ in a 3.7 K ion trap. *Mol. Phys.* **2015**, *113*, 2320−2332.

DOI: 10.1021/acs.jctc.7b01136
J. Chem. Theory Comput. 2018, 14, 1523−1533